JGR Atmospheres

RESEARCH ARTICLE
10.1029/2025JD044251

Environmental Influences on Deep Convective Upscale Growth Rate in Central Argentina From a Convection-Permitting Simulation

Clayton R. S. Sasaki[1], Angela K. Rowe[2], Lynn A. McMurdie[1], Adam C. Varble[3], and Zhixiao Zhang[4]

[1]Department of Atmospheric and Climate Science, University of Washington, Seattle, WA, USA, [2]Department of Atmospheric and Oceanic Sciences, University of Wisconsin-Madison, Madison, WI, USA, [3]Atmospheric, Climate, and Earth Sciences Division, Pacific Northwest National Laboratory, Richland, WA, USA, [4]Department of Physics, University of Oxford, Oxford, UK

Abstract This study uses a convection-permitting model simulation to describe the environmental conditions under which convective upscale growth occurs in central Argentina, particularly examining environmental parameters when deep convection initially forms that could differentiate the rate of initial upscale growth. Simulated mesoscale convective systems (MCSs) are separated into slow and rapid growth by the rate of spatial growth from convection initiation until reaching the MCS scale. A low-level jet (LLJ) is found more frequently near the deep convection that experiences rapid growth to an MCS, but its presence alone is not predictive of rapid growth. Using spatially-averaged parameters, we find that rapid growth to MCSs also occurs in environments that are significantly more thermodynamically favorable with greater low-level moisture and instability. Fewer significant differences are found in the kinematic environment with only the 0–2 km vertical wind shear magnitude being significantly larger for rapid growth MCSs compared to slow growth MCSs, potentially related to LLJs often peaking near this height. When focusing only on MCSs with the slowest and fastest growth rates, elevated-layer shear is significantly smaller for very rapid growth MCSs, suggesting elevated-layer shear may help discriminate between the upper and lower bounds of growth rate. Finally, when upscale growth occurs near the Sierras de Córdoba (SDC) with a LLJ present, rapid growth is also supported by favorable wind shear orientation. However, this does not hold for upscale growth occurring away from the SDC, highlighting the importance of interpreting shear direction relative to the orientation of features initiating deep convection.

Plain Language Summary Understanding the environments that support spatial growth of storms is crucial for predicting their impacts. This study uses a 6.5-month-long high-resolution model simulation to examine the environments of simulated storm systems separated based on their rate of spatial growth. Results show that environments with a faster growth rate have greater moisture and instability. While vertical wind shear, defined as the change in wind speed and/or direction with height, is a well-known factor in storm organization, its magnitude does not vary strongly with growth rate when shear is averaged over a large area, likely due to the large spread in values present. However, the direction of wind shear is likely an important factor in the rate of growth, and faster spatial growth is found for storms growing near the mountains when a favorable shear direction (parallel to the mountain range) is present. A low-level jet, an area of stronger wind speeds elevated off of the surface, is found more frequently in environments with a faster growth rate and is likely an important mechanism that facilitates differences in thermodynamics and wind shear.

Key Points:

- Using a seasonal convection-permitting simulation, environments are compared for storms with slow and rapid spatial growth to mesoscale convective systems (MCS)
- Rapid growth is favored in environments with greater low-level moisture and instability, likely related to the presence of a low-level jet (LLJ)
- Favorable vertical wind shear orientation when a LLJ is present near the mountains likely also supports rapid MCS growth

Supporting Information:

Supporting Information may be found in the online version of this article.

Correspondence to:

A. K. Rowe,
akrowe@wisc.edu

Citation:

Sasaki, C. R. S., Rowe, A. K., McMurdie, L. A., Varble, A. C., & Zhang, Z. (2026). Environmental influences on deep convective upscale growth rate in central Argentina from a convection-permitting simulation. *Journal of Geophysical Research: Atmospheres*, *131*, e2025JD044251. https://doi.org/10.1029/2025JD044251

Received 1 MAY 2025
Accepted 11 DEC 2025

Author Contributions:

Conceptualization: Clayton R. S. Sasaki, Angela K. Rowe, Lynn A. McMurdie
Data curation: Clayton R. S. Sasaki
Formal analysis: Clayton R. S. Sasaki
Funding acquisition: Angela K. Rowe, Lynn A. McMurdie
Investigation: Clayton R. S. Sasaki, Angela K. Rowe
Methodology: Clayton R. S. Sasaki, Angela K. Rowe, Lynn A. McMurdie, Adam C. Varble, Zhixiao Zhang
Resources: Adam C. Varble, Zhixiao Zhang
Software: Clayton R. S. Sasaki

1. Introduction

Convective upscale growth, the collection of processes by which discrete deep convection transitions to large, organized mesoscale convective systems (MCSs), remains difficult to forecast (e.g., Peters et al., 2017; Weisman et al., 2013). An improved understanding of the processes and environments in which upscale growth occurs is necessary to improve forecasting of severe weather hazards which are dependent on the mode of convection (e.g., discrete vs. multicellular; e.g., Trapp et al., 2005; Gallus et al., 2008; Smith et al., 2012). Additionally, MCSs are major contributors to warm-season rainfall and exert significant influence on large-scale atmospheric circulations (Hartmann et al., 1984; Schumacher & Johnson, 2005), further highlighting the need to understand upscale growth environments.

Supervision: Angela K. Rowe, Lynn A. McMurdie
Visualization: Clayton R. S. Sasaki
Writing – original draft: Clayton R. S. Sasaki
Writing – review & editing: Clayton R. S. Sasaki, Angela K. Rowe, Lynn A. McMurdie, Adam C. Varble, Zhixiao Zhang

Idealized modeling, reanalysis, case studies using convection-permitting models, and relatively coarse long-term simulations have all been used to improve our understanding of the large-scale environments which favor upscale growth into MCSs in the mid-latitudes. These environments include the presence of a mid-level trough which promotes synoptic-scale lifting (e.g., Tao & Simpson, 1984; Uccellini & Johnson, 1979), a low-level jet (LLJ) which transports warm, moist air in the low levels, increasing instability (e.g., Rasmusson & Mo, 1996; Wu & Raman, 1998), and a frontal zone which enhances low-level convergence (e.g., Crook & Moncrieff, 1988; Maddox et al., 1979; Peters & Schumacher, 2014). How these large-scale environments that are favorable for convection and its upscale growth imprint on the mesoscale and convective scale environments needs to be better understood to be able to predict the location and timing of MCSs (Thielen & Gallus, 2019). This connection between scales remains less understood, in part owing to the lack of high-resolution spatial and temporal observations.

Previous studies from the U.S. Great Plains have identified a wide variety of parameters that may predict favorable environments for upscale growth (e.g., Coniglio et al., 2010; Hwang et al., 2022; Hwang and Li, 2022; Jirak & Cotton, 2007; Thompson et al., 2012). These include thermodynamic parameters such as strong 700-hPa temperature advection, steep low-level equivalent potential temperature lapse rates, large amounts of convective available potential energy (CAPE), and a small height difference between the level of free convection (LFC) and lifting condensation level (LCL) (LFC-LCL), as well as kinematic parameters such as vertical wind shear, hereafter referred to as wind shear, over a range of height layers (e.g., stronger 0–3 km wind shear, weaker 3–10 km wind shear; e.g., Coniglio et al., 2010). Many studies agree on the importance of the thermodynamic environment but have mixed conclusions on whether vertical wind shear magnitude can discriminate between MCS and non-MCS environments (e.g., Hiris & Gallus, 2021). Coniglio et al. (2010) hypothesized that weaker deep-layer shear creates less favorable conditions for the development of supercells, which could otherwise delay the transition to MCSs, while stronger low-level shear favors enhanced lifting along the gust front and warm air advection and thus faster upscale growth. However, wind shear magnitude might be a better indicator of whether the system produces severe winds (Cohen et al., 2007), while the wind shear vector direction could be predictive of whether convection grows upscale with strong deep-layer shear parallel to the initiating boundary being more favorable for rapid upscale growth (e.g., Dial et al., 2010). Overall, the number of studies which examine differences in environmental conditions based on the rate of initial upscale growth are limited and even fewer studies have explored these conditions in regions with complex terrain.

Central Argentina is a global hotspot of deep convection with convection that initiates near the Sierras de Córdoba (SDC) mountain range prone to rapid upscale growth in the warm season (Feng et al., 2022; Mulholland et al., 2018, 2019; Rocque & Rasmussen, 2022). MCSs in central Argentina often occur when a synoptic trough is located upstream of the Andes Mountains (e.g., Rasmussen & Houze, 2016) and when the South American Low-level Jet (SALLJ) is present (e.g., Salio et al., 2007). This large-scale setup leads to strong deep-layer shear, enhanced instability, and a strong poleward moisture flux with convergence at the terminus of the SALLJ (e.g., Salio et al., 2007). In these cases, deep convection initiation is often focused near the SDC due to subsiding mid-level air creating a capping inversion that is overcome by air lifted over the SDC (e.g., Rasmussen & Houze, 2011). Additionally, both synoptically-driven and diurnally-driven SALLJs have been observed, with the former being longer-lasting and more elevated with less of a diurnal cycle (e.g., Sasaki et al., 2022). However, not all convection that grows upscale occurs in this synoptic environment (e.g., Rocque & Rasmussen, 2022) and less is understood about the mesoscale environment influences on upscale growth.

Studies over the last decade have begun to explore how the convective environment in central Argentina might differ from those found in other regions, particularly in the heavily studied U.S. Great Plains. More specifically, storm environments in central Argentina tend to be characterized by larger CAPE and weaker low-level vertical wind shear than storm environments in the U.S. (Mulholland et al., 2018; Piscitelli et al., 2022; Schumacher, 2021). Case-based high-resolution (<1 km) models have been used to show that a thin ribbon of enhanced deep-layer vertical wind shear and instability exists east of the SDC (Mulholland et al., 2019), and the SALLJ may focus deep convection initiation over the southern portion of the SDC (Sasaki et al., 2024; Singh et al., 2022). The recent 2018–2019 Remote sensing of Electrification, Lightning, and Mesoscale/microscale Processes with Adaptative Ground Observations (RELAMPAGO; Nesbitt et al., 2021) and Cloud, Aerosol, and Complex Terrain Interactions (CACTI; Varble et al., 2021) field campaigns provided some of the most comprehensive observations of convection near the SDC and its environment to date. In addition to providing favorable conditions for deep convection initiation, case studies using these RELAMPAGO observations linked

subsequent upscale growth to the direction of the deep-layer shear vector, which at times was influenced by the SALLJ that occurred over varying heights (Sasaki et al., 2025).

As part of the RELAMPAGO-CACTI campaign, a 6.5-month Weather Research and Forecasting (WRF) model simulation (described in Zhang et al., 2021) was run, capturing a wide spectrum of upscale growth events using convective scale (3-km) horizontal grid spacing to resolve environmental conditions in the context of complex terrain. Using large-scale composites, Zhang et al. (2021) showed that the model approximately reproduced many satellite-observed MCS characteristics. They also found that the model produced previously observed synoptic environments favorable for MCSs, and that MCS growth rate was accelerated with increased favorability in the synoptic environment (e.g., stronger synoptic-scale lift, a stronger thermo-orographic northwestern Argentinean low in the lee of the Andes), although their study did not explicitly identify the SALLJ. This study builds on those results, exploring upscale growth in this region using the 6.5 months of WRF-simulated upscale growth cases to identify initial growth environments across a range of scales and quantify which environmental parameters are linked to area growth rate, including in the context of the SALLJ. Our specific objectives are therefore to (a) identify where and when convection grows upscale in central Argentina, particularly relative to the SDC, (b) quantify the initial environments in which upscale growth occurs, and (c) examine which thermodynamic and kinematic environmental parameters differentiate the rate of initial upscale growth.

2. Data Sources and Methods

2.1. WRF Setup

The simulation used in this analysis was a 6.5-month convection-permitting run of the WRF model (version 4.1.1; Skamarock et al., 2019) covering the October 2018–April 2019 experimental period of the CACTI campaign. The domain was centered over central Argentina, expanding from just west of the Andes Mountains to the Atlantic Ocean in the east, and included the SDC mountain range (Figure 1). To simulate realistic convective evolution, the model had 3-km horizontal grid spacing, 80 vertical levels (stacked in the low-levels to keep vertical grid spacing 250 m or less below 5 km), and 15-min 2-dimensional (2D) output with hourly 3-dimensional (3D) output covering the full domain. Initial and boundary conditions were drawn from the fifth-generation global reanalysis produced by the European Centre for Medium-Range Weather Forecasts (ERA5; Hersbach et al., 2020) and no observation or reanalysis nudging was applied. Physical parameterizations used in the simulation include the Mellor–Yamada–Nakanishi–Niino (MYNN) level-2.5 (Nakanishi & Niino, 2006, 2009) eddy diffusivity mass flux scheme, the Noah land surface scheme (Tewari et al., 2004), the Eta Similarity surface layer scheme (Janjić, 1994; Monin & Obukhov, 1954), and the Rapid Radiative Transfer Model for General Circulation Models (RRTMG; Iacono et al., 2008) with aerosol interactions turned on. Additionally, the Thompson aerosol aware scheme was used with aerosol number concentrations based on climatology for this region (Thompson & Eidhammer, 2014).

Further details of this model setup are found in Zhang et al. (2021), which determined that the model accurately reproduced the seasonal and diurnal distributions of satellite-observed MCSs, including their maximum cloud shield areas, rainfall volumes, and minimum top-of-atmosphere infrared brightness temperatures (TOA IR T_b). However, the model overestimated MCS propagation speeds and produced larger heavy rain ratios (i.e., overestimated convective rainfall in comparison to stratiform), validated with surface radar measurements in Zhang et al. (2024), which is a common issue across a variety of convection-permitting model setups (Feng et al., 2025). Additional work by Sasaki et al. (2024) validated the representation of the modeled SALLJ and found that it had similar characteristics to the observed SALLJ with low-level winds close to the higher terrain slightly underestimated in WRF. These results supported using this model simulation to investigate the environmental conditions that control initial upscale growth.

2.2. MCS Tracks and Characteristics

Deep convective systems were tracked in the model using the PyFLEXTRKR software (Feng et al., 2023) and simulated TOA IR T_b, beginning when a cold cloud core ($T_b < 225$ K) was identified. The cold cloud shield area (CCS area; $T_b < 241$ K) was then saved every half an hour for systems that reached MCS thresholds during their lifecycle. To be considered an MCS, the tracked system was required to have a CCS area larger than 10,000 km^2 and contain a precipitation feature with a major axis length >100 km that lasted for at least 2 hr (Zhang et al., 2021). For each tracked simulated MCS, "first storms" and "initiation" stages were defined separately. The

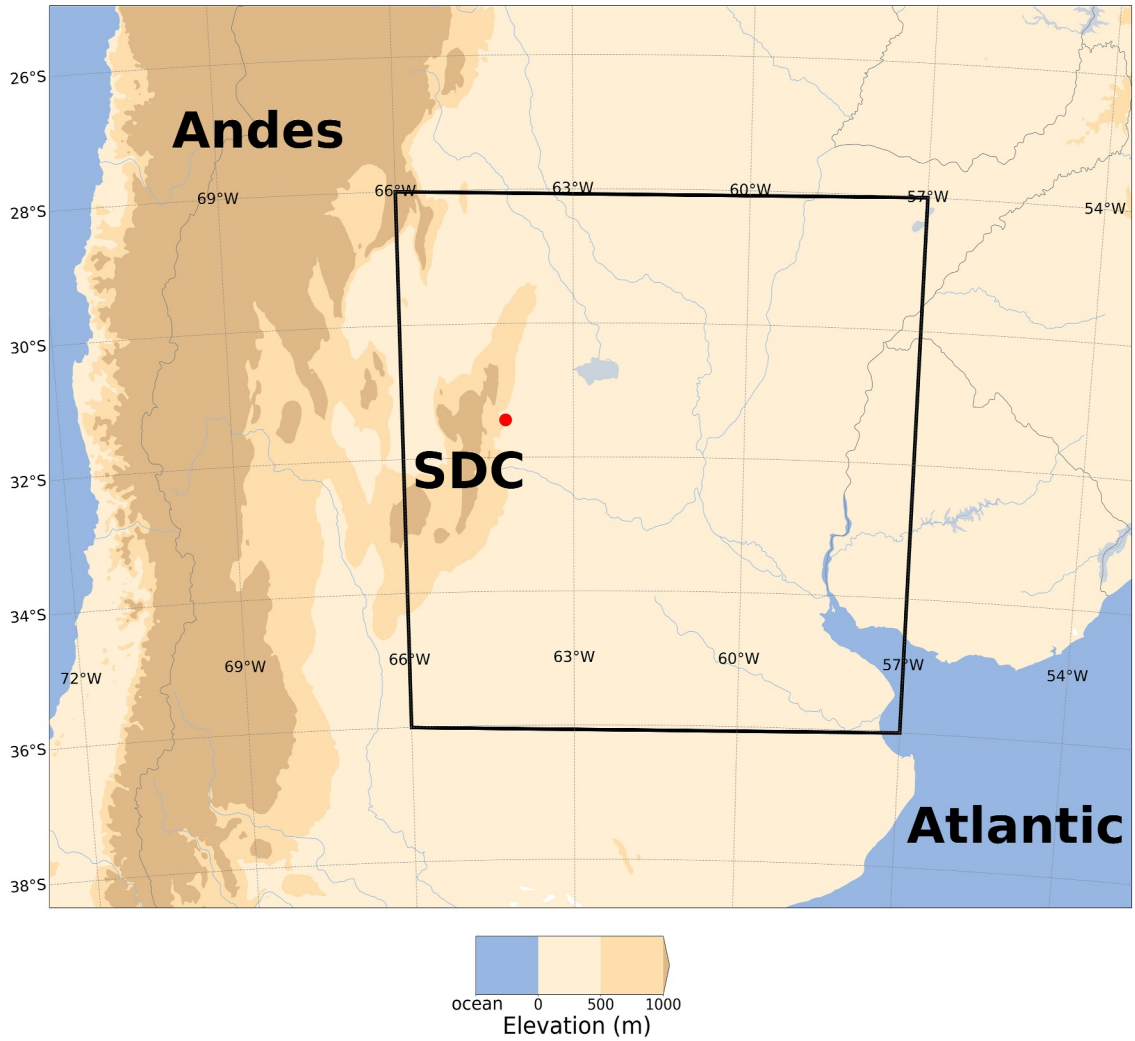

Figure 1. Map of Weather Research and Forecasting domain with the region considered for tracked mesoscale convective systems "first storms" locations outlined in black. The topography (beige filled contours) is shown in 500-m increments along with the location of Córdoba (red dot).

"first storms" stage was defined as the earliest output time at which a trackable convective object was detected (i.e., a cold cloud core), and the "MCS initiation" stage was the first output time where the tracked object met the MCS criteria above. At both stages the CCS area was saved and an "initial growth rate" was calculated based on the difference in the CCS areas divided by the time difference (hours between the two defined stages). The tracked MCSs were separated into two groups based on the initial growth rate and this separation is discussed in the Results section. Note that this growth rate was defined during the MCS developing stage (i.e., pre-MCS) and the environments were quantified at the "first storms" time, rather than during the subsequent evolution of the MCS.

Our analysis uses tracked MCSs with "first storms" locations near and east of the SDC (black-outlined rectangle in Figure 1), where environmental conditions could be calculated using model output. Convective objects that met the MCS size criteria could either be produced by new tracked objects growing in area or the splitting/merging of tracked objects that already met the MCS criteria. We removed those that resulted from the splitting or merging of pre-existing MCSs as this study is focused on initial growth of smaller convective cells into MCSs. A total of 137 MCSs met the established criteria, at times with multiple MCSs on a given day, and were included in our analysis.

2.3. Environmental Conditions and SALLJ Characteristics

To understand the environmental conditions impacting initial upscale growth of convection, environmental parameters were calculated from 3D WRF output at the time of the "first storms" stage for each tracked simulated

MCS. As the 3D output was saved hourly and the 2D MCS characteristics (i.e., top-of-atmosphere OLR, rain rate) were saved every 30 min, the closest hourly WRF file before the "first storms" time was used.

Several thermodynamic and kinematic parameters related to various aspects of deep convection initiation and mesoscale organization were calculated with a particular focus on those used for quantifying low-level jets and those highlighted in past studies of upscale growth events (e.g., Coniglio et al., 2010; Mulholland et al., 2018; Sasaki et al., 2024). Those parameters were: 850-hPa specific humidity and meridional specific humidity flux, most-unstable and lowest 100-hPa mixed-layer CAPE (MUCAPE, MLCAPE), low-level (500–3,000 m AGL) equivalent potential temperature lapse rate, LCL, LFC, and differences between upper- and lower-level horizontal wind vectors (hereafter "wind shear"). Wind shear was calculated over standard surface-based layers (e.g., 0–6 km), layers that have been hypothesized to be specifically applicable to upscale growth environments (e.g., 3–10 km), along with layers that capture the shear associated with the varying height of the SALLJ (e.g., 2–6 km; Sasaki et al., 2024, 2025). Convective available potential energy, convective inhibition (CIN), LCL, and LFC were all computed using the cape_2d routine in the wrf-python package (Ladwig, 2017), which pseudoadiabatically lifts a mean parcel within a 500-m layer centered on the maximum equivalent potential temperature in the lowest 3,000 m and incorporates the virtual temperature correction.

Additionally, we explored parameters which have received less widespread use in predicting upscale growth. Idealized large-eddy simulations have shown that when the LFC-LCL height difference is small, deep moist convection becomes more likely (Kang & Bryan, 2011). Most studies of the LFC-LCL height difference have been focused on convection initiation, but recently a couple studies have found this parameter to be a useful predictor of MCS characteristics (e.g., duration; Hwang and Li, 2022; Hwang et al., 2022). Additionally, a recent study showed that higher LCL heights were related to wider and deeper updrafts along with stronger vertical velocities among simulations with similar CAPE (Mulholland et al., 2021). These higher LCL heights could lead to more sub-cloud evaporation, stronger cold pools, and potentially more rapid upscale convective growth via cold pool merging.

Environmental conditions were averaged over a 4° by 4° region centered on the "first storms" centroid location. The size of this area was chosen to capture the impact of the meso-β to synoptic-scale environment, including the SDC, and was similarly sized to domains used in previous studies characterizing environmental conditions of MCSs, in both the U.S. and South America (Coniglio et al., 2010; Hwang et al., 2022; Hwang and Li, 2022; Mulholland et al., 2018).

The SALLJ was objectively identified using the criteria from Sasaki et al. (2022): a horizontal wind maximum >12 m s^{-1} within 3,200 m AGL and a decrease >6 m s^{-1} to the first minimum or 5,700 m AGL. The region used for SALLJ calculations (i.e., SALLJ areal coverage, height, and strength) was a 2° latitude by 4° longitude region with the bottom edge offset 1° north of the "first storms" centroid. This area was shifted north of the centroid to better identify SALLJs potentially influencing the convection even when the low-level environmental winds in-and-around the convection were disrupted by convection at the "first storms" stage. An event was counted as having a SALLJ present if a SALLJ was identified in >30% of the defined region, similar to Sasaki et al. (2024) and Du et al. (2014).

To evaluate if statistically significant differences exist between the mean environmental conditions of the growth-rate-separated MCSs, the nonparametric Wilcoxon–Mann–Whitney test was applied. This significance test has been used in many other studies attempting to differentiate between environmental conditions (e.g., Cohen et al., 2007; Coniglio et al., 2010) as nonparametric tests do not require an assumption of the distribution of the data sample and therefore are appropriate in situations with relatively small sample sizes. For this study, a p-value of less than 0.05 (5%) was chosen to indicate statistical significance resulting in a 95% confidence interval.

3. Results

3.1. Growth Locations and Characteristics

As described in the previous section, 137 MCSs were tracked near and east of the SDC, with their "first storms" centroid locations shown in Figure 2a (black stars) along with the corresponding "MCS initiation" centroid locations (gray stars). Both location groupings are concentrated near the southern end of the SDC with ∼22% of "first storms" locations and ∼16% of MCSs initiating over the terrain of the SDC (>500 m MSL). This placement is similar to observations from the Córdoba radar (31.44°S, 64.19°W; Mulholland et al., 2018), but shifted farther

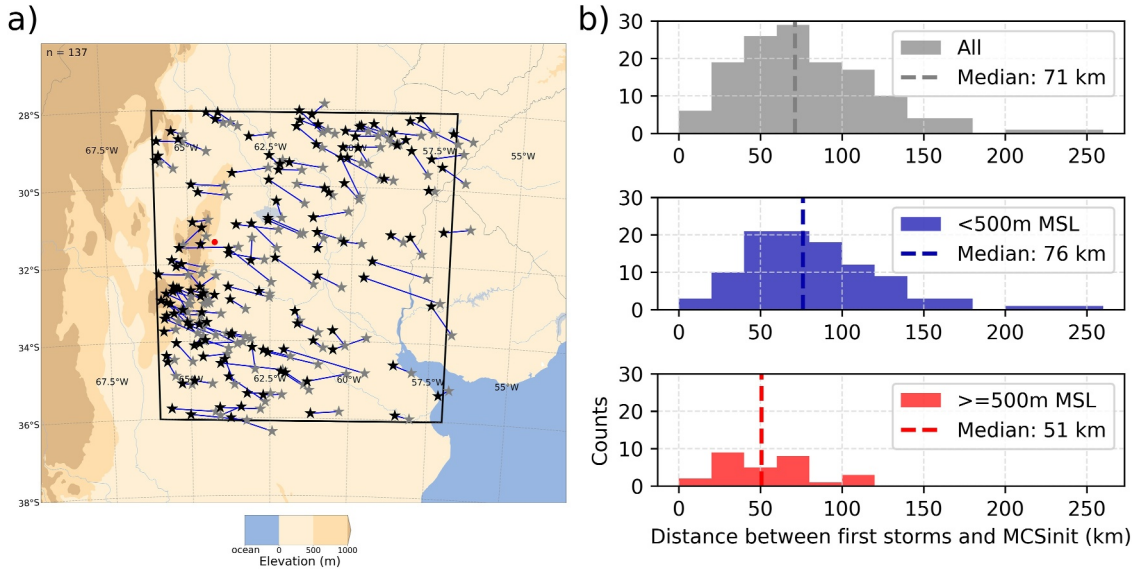

Figure 2. (a) Map of the "first storms" (black stars) and "MCS initiation" (gray stars) locations along with the distance between those locations (blue lines) for each tracked mesoscale convective system (MCS) with map definitions following Figure 1, including Córdoba (red dot). (b) Histograms of the distance between the "first storms" and "MCS initiation" locations for all tracked MCSs (gray), those with "first storms" locations below 500 m MSL (blue), and those with "first storms" locations >500 m (red) MSL.

south and west (i.e., toward higher elevations). This increased modeled frequency over the western portion of the SDC could be related to inter-annual variability, but also suggests that more storms may form there than observed by the terrain-blocked Córdoba radar. Generally, "MCS initiation" locations are located east of the "first storms" locations, but many MCS form near or over the higher terrain of the SDC (>500 m MSL).

The transition from "first storms" to "MCS initiation" occurs over a median distance of 71 km (Figure 2b). This distance is much shorter than that in the Central U.S. (Coniglio et al., 2010), but slightly longer than those found from Córdoba radar observations near the SDC (Mulholland et al., 2018). To understand the discrepancy between the model and observations, the tracks were separated by the elevation of the "first storms" location. In the model, the median distance between the "first storms" and "MCS initiation" locations is 51 km for those where the "first storms" were over the terrain of SDC (>500 m) compared to 76 km for those that began over the lower elevations (Figure 2b). This difference suggests that convection which begins over the SDC grows upscale into an MCS over a shorter distance compared to convection over the lower elevations. This supports previous work that has shown a favorable environment for upscale growth just east of the SDC ridgeline (Singh et al., 2022; Trapp et al., 2020).

The growth times (i.e., the time between "first storms" and "MCS initiation") show further evidence of a quick transition to MCS with a median growth time of 1.5 hr (Figure 3a). Growth times in this study are shorter than prior studies (~2.5 hr; Mulholland et al., 2018) and likely underestimate the total growth time because the initial time used in this study is the time of "first storms", defined as the first output time with a trackable object (based on TOA IR T_b). In comparison, Mulholland et al. (2018) defined a time of convection initiation based on a reflectivity threshold. Further, we define a growth rate as the rate of change in the CCS area over this growth period. Most of the growth rates are below 15,000 $km^2\ hr^{-1}$ with a median rate of 7,700 $km^2\ hr^{-1}$, but the distribution has a long tail with growth rates as high as 30,000 $km^2\ hr^{-1}$ (Figure 3b). To understand what controls the CCS area growth rate, we examine the environmental conditions at the time of "first storms" in the next section.

3.2. Environmental Factors in the Rate of Upscale Growth

Environmental conditions that may impact the rate of the transition from initial cells to an MCS were examined by comparing the environments of those growing rapidly to those that grew more slowly. These environmental conditions were calculated at the "first storms" stage with slow and rapid growth groups separated by the median growth rate (7,700 $km^2\ hr^{-1}$) resulting in 67 slow growth MCSs and 70 rapid growth MCSs. Before showing the

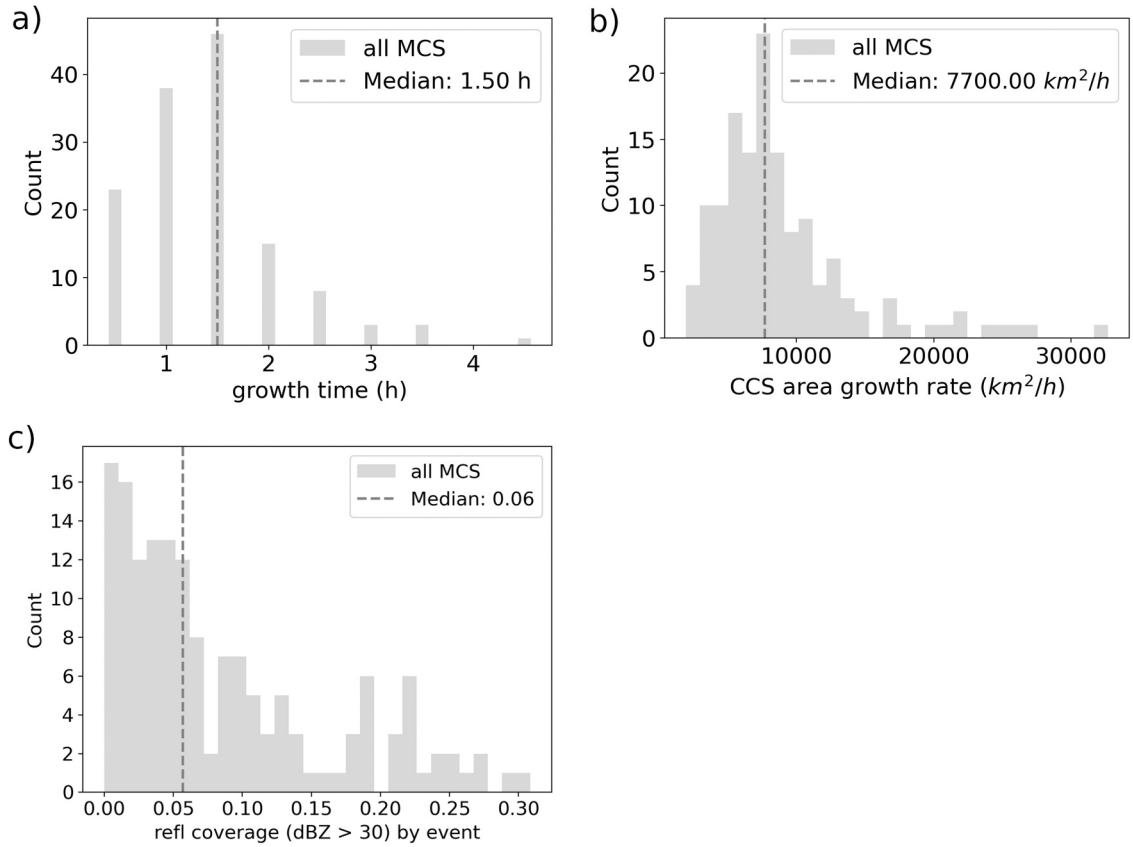

Figure 3. Histograms of (a) growth time, (b) cold cloud shield area growth rate, and (c) the proportion of the area used for identifying the "first storms" environment covered by reflectivity.

environmental conditions, we confirm that the area used for calculating environmental conditions was not contaminated by deep convection. Figure 3c shows the proportion of the area used to calculate these environmental conditions that is covered by reflectivity >30 dBZ. Despite a few cases with coverage >20%, most are generally low at this stage with median convective coverage <6%. Therefore, contamination of the environmental conditions by convection is not a major concern at this early stage of growth, and our results do not vary when recomputing the model environmental fields after excluding all grid points with reflectivity >0 dBZ (see Figures S1–S13 provided in Supporting Information S1).

The "first storms" centroid locations and diurnal frequency separated by growth rate are shown in Figures 4 and 5, respectively. There is no discernible difference in spatial pattern with both slow and rapid growth MCSs occurring over the SDC and over the plains; however, more rapid growth occurred overnight. The temporal distribution broadly follows a bimodal structure with the first and largest peak occurring in the afternoon hours (16:00–22:00 UTC; 13:00–19:00 local time) and a secondary maximum overnight (02:00–06:00 UTC; 23:00–03:00 local time; Figure 5). This general distribution has been found in past studies (e.g., Mulholland et al., 2018; Salio et al., 2007) linking the afternoon peak in deep convection initiation not directly to the time of peak surface heating, but rather to the subsequent period when CIN is minimized and CAPE is maximized (Figure 7c in Varble et al., 2021). The overnight maximum is related to the presence of the nocturnal acceleration of the SALLJ (e.g., Nicolini et al., 2004) near the SDC. This secondary peak in "first storms" times is not present in the U.S. (Coniglio et al., 2010) and likely results from the SALLJ producing convergence and convection initiation along the ridgeline of the SDC (Singh et al., 2022), which grows upscale in the favorable environment just east of the SDC (Mulholland et al., 2019; Trapp et al., 2020).

While the timing of the maxima and minima are similar between rapid and slow growth MCSs, their distributions have differences (Figure 5). For rapid growth MCSs, the afternoon peak is shifted a bit later, possibly associated with the beginning of the strengthening of the SALLJ (Sasaki et al., 2022). Additionally, rapid growth MCSs have

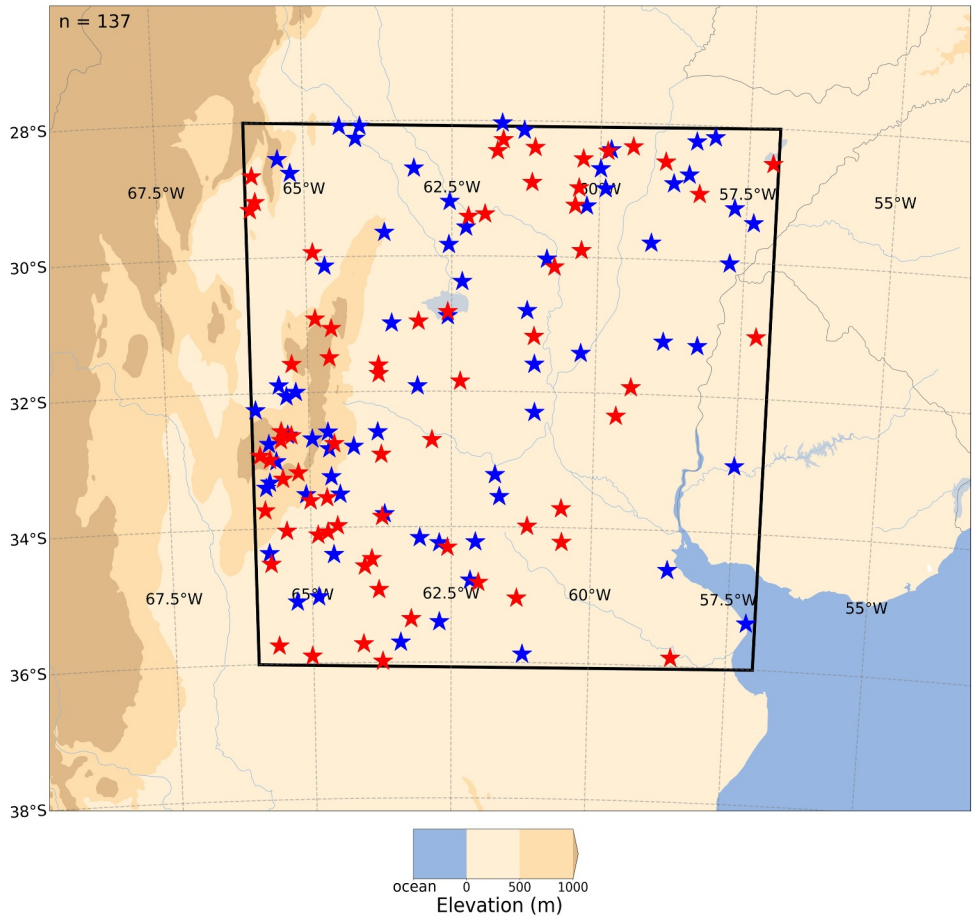

Figure 4. Map of the locations of the "first storms" for rapid growth (blue) and slow growth mesoscale convective systems (red). Elevation is contoured as in Figures 1 and 2.

a narrower secondary peak between 0200 and 0600 UTC, likely linked to favorable conditions produced by the SALLJ, while the peak is broader (almost an extension from the afternoon peak) and much lesser in magnitude for slow growth MCSs. Both growth categories have a distinct minimum in the morning hours.

3.2.1. Low-Level Moisture and Thermodynamic Instability

At the "first storms" time, a higher proportion of rapid growth MCSs have a SALLJ present (36 out of 70, ∼51%) compared to slow growth MCSs (18 out of 67, ∼27%), indicating that the presence of the SALLJ might make

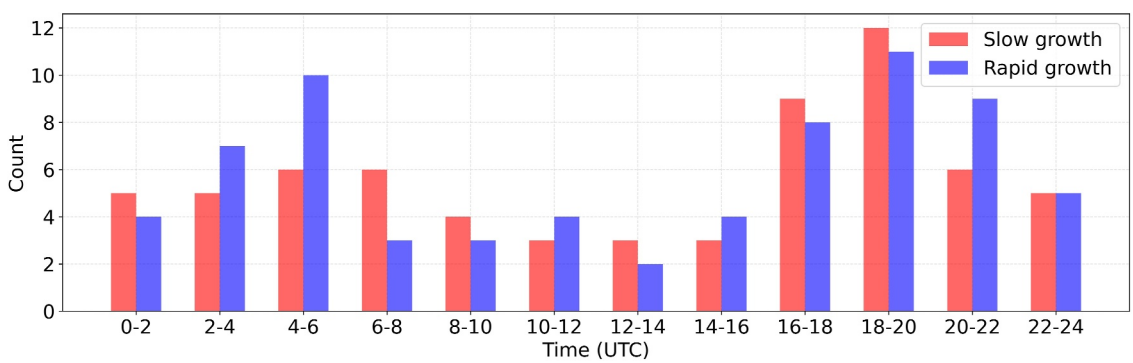

Figure 5. Histograms of the time of the "first storms" for rapid growth (blue) and slow growth mesoscale convective systems (red). Note that local time is UTC–3 hr.

Table 1
SALLJ Counts (in Percentages of Total Counts for Individual Growth Categories) and Median SALLJ Characteristics for Slow and Rapid Growth MCSs at the "First Storms" Stage

	Slow growth (n = 67)	Rapid growth (n = 70)
SALLJ occurrence (% of n)	27 [28]	51 [71]
Median SALLJ max wind (kts)	28	30
Median SALLJ height (m)	1,500	1,500

Note. Numbers in brackets are SALLJ percentages when allowing a SALLJ to be found for any time in the growth stage.

rapid growth more likely (Table 1). However, the presence of a SALLJ at the "first storms" stage alone is neither necessary nor sufficient to indicate rapid growth. When allowing for a SALLJ to be identified at any point during the growth period, instead of just the "first storms" time, the proportion of rapid growth MCSs that have a SALLJ present increases (50 out of 70, ∼71%), but the same conclusion holds that not all rapid growth MCSs have a SALLJ identified during the growth stage. Additionally, characteristics of SALLJs for slow and rapid growth MCSs are similar with no difference in median height, but rapid growth MCSs have a slightly stronger (∼2 kts or 7.5%; or ∼1.03 m s^{-1} as 1 kt ≈ 0.51 m s^{-1}) median SALLJ maximum wind speed. Most (16 out of 20, 80%) of the rapid growth MCSs with a "first storms" time between 02:00 and 08:00 UTC, had a SALLJ present (not shown), further highlighting the impact of the nocturnal acceleration of the SALLJ on upscale growth.

Rapid growth MCSs are associated with a more favorable thermodynamic environment (Figure 6), likely influenced by the SALLJ (Sasaki et al., 2024). Median specific humidity at 850 hPa is 10.9 g kg^{-1} for all MCS events with significantly larger values found during rapid growth MCSs (11.2 g kg^{-1}) compared to slow growth MCSs (10.4 g kg^{-1}; Figure 6a). Similarly, rapid growth MCSs have a significantly stronger meridional flux of specific humidity. The median value is −49.1 g kg^{-1} m s^{-1} for rapid growth MCSs and −19.2 g kg^{-1} m s^{-1} for slow growth MCSs (Figure 6b), with the greatest values within each growth category associated with periods when the SALLJ was present compared to those when it was not (see subdivided figures for each thermodynamic variable in Supporting Information S1 as Figures S22–S29 in Supporting Information S1). Together these results align with the more frequent and stronger SALLJ present during rapid growth MCSs (Table 1). This result is supported by prior work which showed larger values of low-level moisture near the SDC during periods when the SALLJ was present (Sasaki et al., 2024).

Environments of rapid growth MCSs also have significantly larger conditional instability for updraft parcels (Figures 6c and 6d). Median MLCAPE (MUCAPE) values are 867 (1,202) J kg^{-1} for rapid growth MCSs compared to 468 (918) J kg^{-1} for slow growth MCSs. The significant difference between the slow and rapid growth MCSs for both the most-unstable and mixed-layer parcels suggests that a deep layer of greater instability is present in the environments of rapid growth MCSs, which is aligned with past studies that have found deep SALLJs influencing the thermodynamic environment over a wide range of heights (e.g., Sasaki et al., 2022). The larger spatially averaged CAPE value supports past work which has described a spatially broad area of instability during rapid growth MCSs (Zhang et al., 2021) and particularly large values when the SALLJ is present (Sasaki et al., 2024), although additional factors such as the diurnal cycle should be taken into consideration where CAPE may be lower during overnight periods of rapid growth when the SALLJ is present. The median CAPE values for all MCS events are similar to those from a study that used reanalysis in this region (Mulholland et al., 2018) and also MCS environments analyzed by Thompson et al. (2012) in the U.S.

The larger CAPE is a result of greater low-level equivalent potential temperature (θ_e), and the differences in the profile of θ_e can be seen when comparing potential instability ($\partial\theta_e/\partial z$), which shows significantly larger magnitudes for the rapid growth MCSs (Figure 6e). Large decreases in θ_e with height (potential instability) can indicate an environment that is favorable for slab lifting which can lead to rapid destabilization when whole layers undergo strong lifting. This strong lifting can come from many sources including low-level jets and terrain (e.g., Du et al., 2020; French & Parker, 2010), both of which are found in this region. Additionally, a rapid expansion of convection along the cold pool edge can occur in this type of environment when strong cold pools and significant line-normal wind shear are present, leading to enhanced lifting (Coniglio et al., 2010; Du et al., 2020).

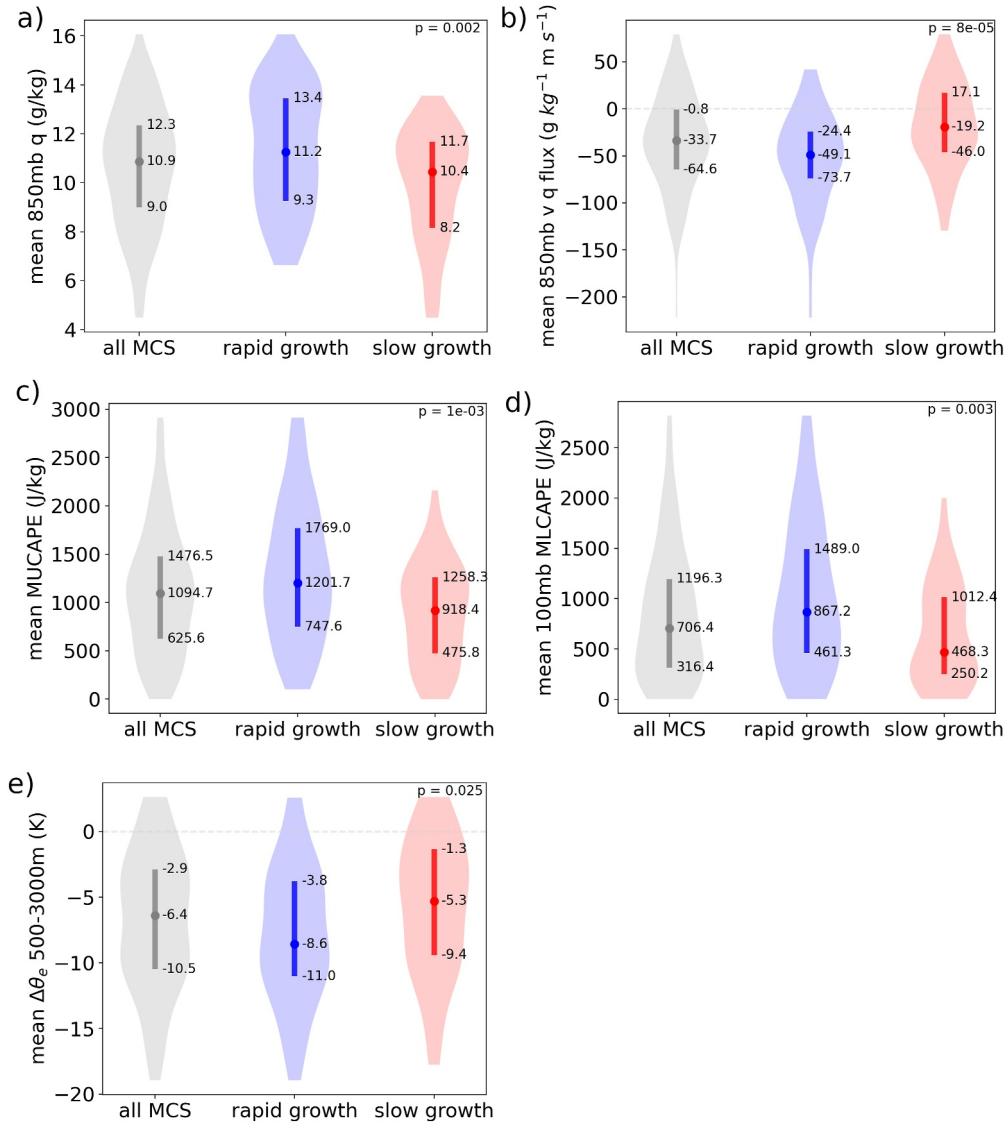

Figure 6. Violin plots showing the distributions of the spatially averaged thermodynamic environment at the "first storms" stage for all mesoscale convective systems (MCSs) (gray), rapid growth MCSs (blue), and slow growth MCSs (red). The variables shown are (a) 850-hPa specific humidity, (b) 850-hPa meridional specific humidity flux, (c) MUCAPE, (d) MLCAPE, and (e) the difference in equivalent potential temperature (θ_e) between 500 and 3,000 m AGL. The median along with the 25th and 75th percentile values are shown. P-values from the Mann–Whitney test are used to determine statistical significance between rapid and slow growth distributions.

3.2.2. Inhibition Depth and Cloud Base

The height difference between the LFC and LCL is a measure of the depth of the CIN layer. LFC-LCL values were found to be significantly smaller for environments with rapid growth MCSs compared to those with slow growth MCSs (Figure 7a). A smaller inhibition depth could allow convection to develop with weaker ascent, allowing convection to form over a wider area for a given forcing. Less inhibition may also result in weaker convection that is more widespread (Bennett et al., 2006; Browning et al., 2007; Russell et al., 2008) and more cells closer to one another where the cold pools could merge and grow upscale (e.g., Peters et al., 2017).

Both LFC and LCL heights are significantly lower for rapid growth MCSs compared to slow growth MCSs (Figures 7b and 7c) with lower LFC heights contributing more to the smaller LFC-LCL difference. Level of free convection heights are ∼24% higher and LCL heights are ∼15% higher during slow growth MCSs compared to rapid growth MCSs. The lower LFC heights and shallower inhibition layers (LFC-LCL) during rapid growth

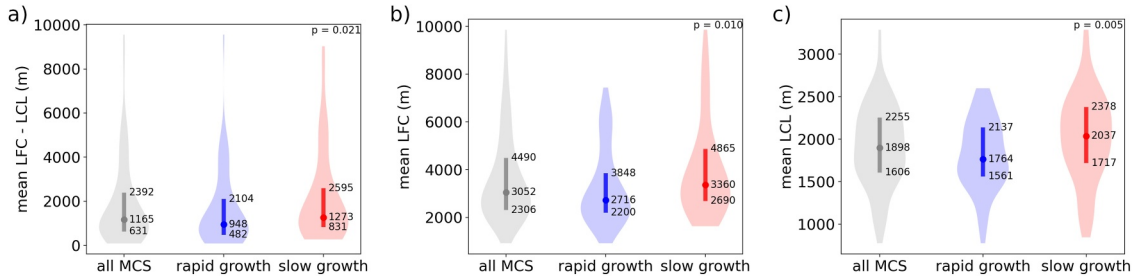

Figure 7. As in Figure 6, but the variables shown are (a) the height difference between the level of free convection (LFC) and lifting condensation level (LCL), (b) the LFC height and, (c) the LCL height.

MCSs may allow thunderstorms to be more easily initiated and maintained (Davies, 2004). Generally, LCL heights during MCS events are higher in South America compared to the U.S. (Garcia et al., 2024; Ribeiro & Bosart, 2018; Thompson et al., 2012), which have been linked to stronger updrafts (e.g., Mulholland et al., 2021). It has also been hypothesized that these higher LCL heights may produce more rapid convective upscale growth through increased sub-cloud evaporation leading to stronger and deeper cold pools and more merging of cold pools (Mulholland et al., 2018). However, sub-cloud evaporative cooling is also strongly linked to the specific humidity, which is higher for rapid growth MCSs (Figure 6a). Therefore, the LCL heights being found to be slightly lower for rapid growth MCSs (Figure 7c) points to the likely more important role of specific humidity in this distinction between growth rate. There could also be other mechanisms playing a role, such as strong cold pools leading to shear-cold pool circulation imbalances providing suboptimal updraft forcing (e.g., Rotunno et al., 1988).

3.2.3. Vertical Wind Shear Magnitudes

Shear magnitudes over various height layers were investigated using similar methods described in the previous subsections. Generally, shear magnitude does not appear to be a good discriminator between slow and rapid MCS growth rates with no significant differences (p-values >0.05) found and median value differences of less than 3 kts for all layers except for 0–2 km shear (Figure 8). The significantly larger 0–2 km shear for rapid growth MCSs is linked, in part, to the more frequent presence of the SALLJ (Table 1), with greater shear magnitudes during rapid growth periods with the SALLJ compared to without (see Figures S30–S34 in Supporting Information S1), and could indicate an environment that is favorable for the triggering of initial convection by cold pools (Rotunno et al., 1988). Long-duration, deep (~2.5 km) cold pools have been found in Central Argentina (Schumacher, 2021), and modeling studies (e.g., Mulholland et al., 2019) have shown that the terrain of the SDC can block and deepen these cold pools. While the differences are not significant, the median 0–3 km shear is also larger for rapid growth MCSs compared to slow growth. A hypothesis for this stronger low-level shear during rapid growth is that cold pools in this sheared environment trigger new convection through low-level wind shear optimally balancing the cold pool circulation promoting deep ascent (i.e., RKW theory; Rotunno et al., 1988), which may be contributing to a rapid increase in the cloud area and therefore a faster area growth rate.

Median deep layer (0–6 km) wind shear magnitudes are similar (~39 kts) between slow and rapid growth MCSs and do not show significant differences. This result suggests that deep-layer shear likely does not control growth rate and is therefore not a good discriminator between these environments. The median 0–6 km shear values are also of similar magnitude to those found during MCS events in the U.S. (Thompson et al., 2012). The median shear magnitudes for elevated layers (2–6 km, 3–10 km; Figures 8d and 8e) also do not show significant differences between rapid growth and slow growth MCSs; however, the median values are slightly lower for rapid growth MCSs. These differences are consistent in sign with U.S.-based reanalysis studies which have shown smaller magnitudes of 3–10 km shear for rapid growth MCSs (e.g., Coniglio et al., 2010) and idealized simulations showing that environments with more of the total wind shear confined to the low levels favors triggering of convection along a spreading cold pool (e.g., Weisman & Rotunno, 2004). Furthermore, previous research has shown that rapid growth frequently occurs in scenarios with strong synoptic forcing (e.g., Rocque & Rasmussen, 2022; Sasaki et al., 2025; Zhang et al., 2021), characterized by strong winds aloft within the trough. These strong winds aloft when a SALLJ is present can result in weaker shear magnitudes over elevated layers, as was the case on 17 November in the simulations when strong mid-level winds in the presence of a strong SALLJ led to

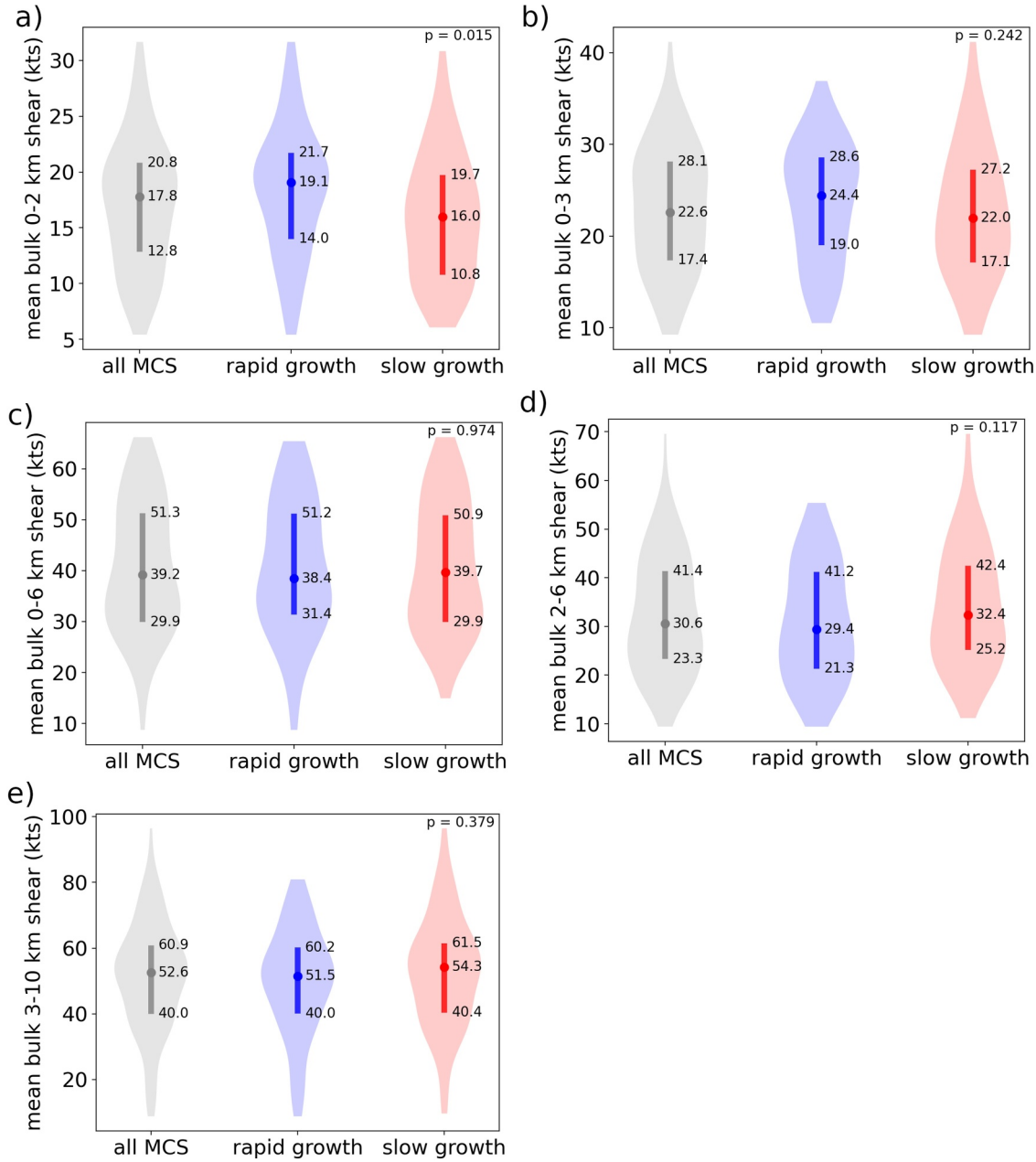

Figure 8. As in Figure 6, but showing bulk wind shear for (a) 0–2 km, (b) 0–3 km, (c) 0–6 km, (d) 2–6 km, and (e) 3–10 km.

mean 2–6 km shear values of 19.49 kts (not shown) and in the narrow spread of shear values when a SALLJ was present during rapid growth periods (see Figures S31–S34 in Supporting Information S1). The strength and orientation of the winds both matter for the 2–6-km shear magnitude and contribute to the variability.

The lack of statistically significant differences between growth rate groups may also be influenced by the choice of threshold used to define the groups. Therefore, two new groups with greater separation were created using the median growth rate ±0.5 standard deviation, leading to very slow growth MCSs ($\leq$5,078 km^2 hr^{-1}) and very rapid growth MCSs ($\geq$10,322 km^2 hr^{-1}). With these new groups (Figure 9), the conclusions from the previous analysis generally hold, with one notable exception: the 2–6 and 3–10 km shear is now significantly smaller for very rapid growth MCSs compared to very slow growth MCSs. Again, this aligns with work from the U.S. (Coniglio et al., 2010), suggesting that weaker elevated-layer shear is a good discriminator between the upper and lower bounds of the growth rate. The significant differences in these more distinct groups, but not in the median growth-

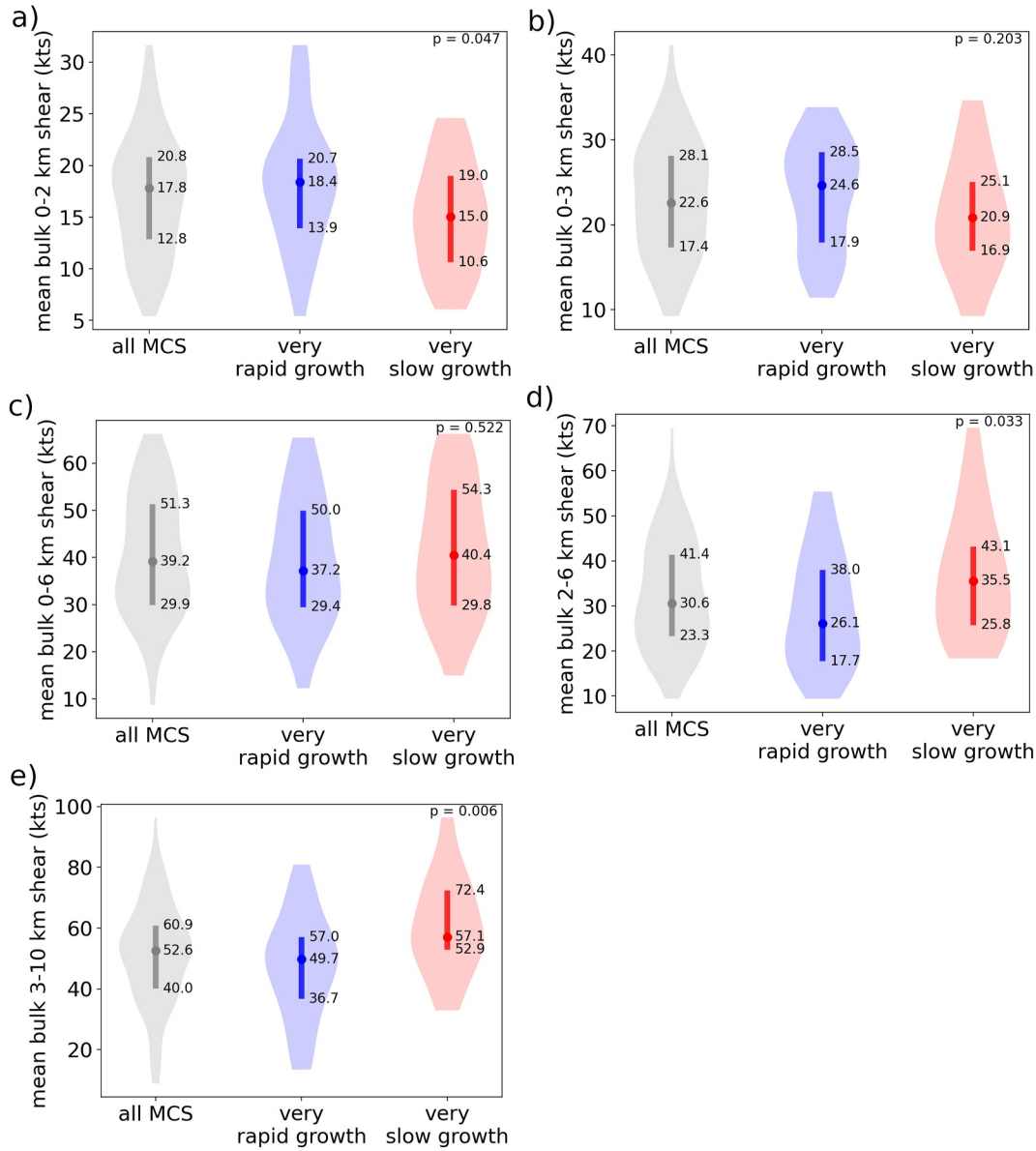

Figure 9. Same as Figure 8 but for the very slow (red) and very rapid (blue) growth mesoscale convective systems.

separated groups including all cases, suggest that while elevated-layer shear can help distinguish between the extremes of MCS growth rates, its influence becomes less clear when considering more moderate or marginal variations in growth. A similar extreme separation was conducted for the thermodynamic variables (see the Figures S14–S21 in Supporting Information S1), with results showing some variables having more significant differences, others less, but overall the main conclusions holding.

Other studies have found mixed results regarding whether shear magnitude can discriminate MCS environments or their resulting characteristics (e.g., Hiris & Gallus, 2021; Hwang et al., 2022; Hwang and Li, 2022). Wind shear differences are likely more complicated than can be portrayed with simple spatial averages, and wind shear values exhibited a larger spatial spread than most thermodynamics parameters investigated, suggesting that the manner in which shear is sampled may affect results. As an example, the distributions of spatial spread (i.e., maximum–minimum values) for 0–3 km wind shear and 850 hPa specific humidity are shown in Figure 10. For 0–3 km wind shear, the median difference between the maximum and minimum value for an MCS event (57.0 kts) is about ~2.5X the median spatially averaged value (22.6 kts). For 850 hPa specific humidity, the median difference

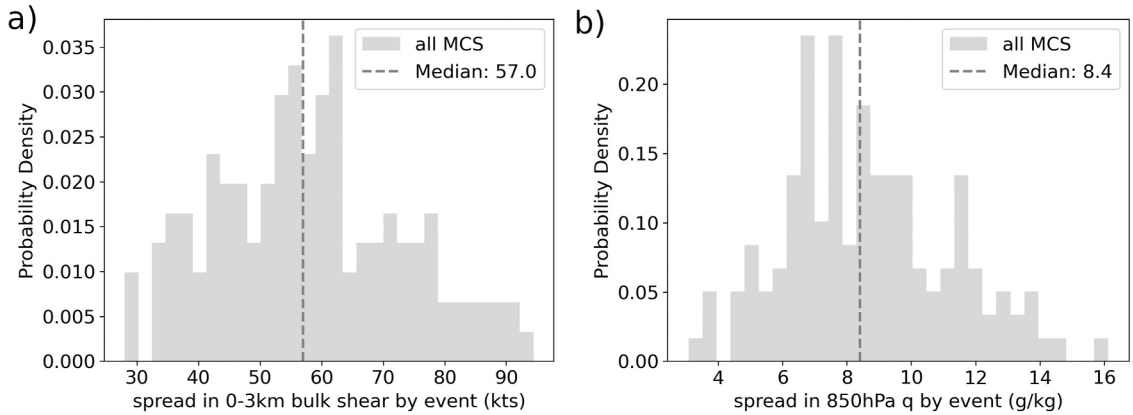

Figure 10. Probability distributions showing the spatial spread for example, kinematic and thermodynamic variables: (a) 0–3 km bulk shear and (b) 850-hPa specific humidity.

between the maximum and minimum value for an MCS event (8.4 g kg^{-1}) is about ∼0.77X the median spatially averaged value (10.9 g kg^{-1}). During the simulated MCS events, the spatial patterns of vertical wind shear were often complex with strong gradients and mesoscale variability present (not shown), suggesting influences on sub-synoptic scales including terrain effects and frontal systems.

While not disproving the importance of spatial patterns, the sensitivity of results to the spatial averaging and size of the region used were tested, with results remaining similar across tests. The sensitivity of the results to the size of the region used was examined by running the same analysis using smaller regions (1.5° by 1.5° and 2° by 2°) which yielded similar results (not shown). Additionally, the sensitivity to the use of averaging was evaluated using an all-points approach, which considered every data point from each event instead of just the mean value. This approach resulted in slightly larger differences between the growth-rate separated MCSs but also a larger spread leading to similar p-values and therefore generally similar results. These sensitivity tests provide confidence that these choices do not substantially impact the results.

3.2.4. Vertical Wind Shear Vector Direction

In addition to shear magnitude, wind shear direction likely impacts the rate of upscale growth with deep-layer shear parallel to the initiating boundary (e.g., frontal boundary, mountain barriers) being more favorable for upscale growth. With this shear direction, storms tend to stay near the area of forcing (e.g., front or terrain) and cold pool merging is promoted due to the along-line/upstream distributions of hydrometeors (e.g., Dial et al., 2010). Past work from this region has shown that the SALLJ can impact the shear direction with both deep- and low-level wind shear being more parallel to the SDC when the SALLJ is present (Sasaki et al., 2024, 2025) that could promote faster upscale growth of terrain-initiated convection.

To investigate this point, Figure 11 is a spatial map of the "first storms" locations separated between the slow and rapid growth MCSs with the presence of the SALLJ shown in context of the 0-3- and 2-6-km vertical wind shear direction. Not only do a higher percentage of the rapid growth MCSs have a SALLJ identified (shown earlier in Table 1), but the difference in SALLJ occurrence is greater for those events that form over the SDC. Of MCSs with "first storms" locations over the SDC (>500 m MSL), a majority (8 out of 14, ∼57%) of the rapid growth have a SALLJ identified (circles in Figure 11, bottom) while none of the slow growth MCSs do (stars in Figure 11, top). Additionally, the rapid growth MCSs with SALLJs identified are focused near the southern end of the SDC, potentially associated with enhanced convergence due to flow-splitting of the SALLJ around the SDC (Sasaki et al., 2024; Singh et al., 2022). These results suggest that the presence of the SALLJ near the SDC indicates a high likelihood of a rapid growth MCS.

Focusing on the 0-3-km shear vector direction (Figure 11, left), many (but not all) of the rapid growth MCSs near the SDC (>500 m MSL) have a northerly shear direction. More specifically, of rapid growth MCSs where the "first storms" location is >500 m, 10 out of 14 (∼71%) have a northerly shear vector. However, similar to the rapid growth MCSs, 10 out of 13 (∼77%) slow growth MCSs have a northerly/southerly shear vector; therefore,

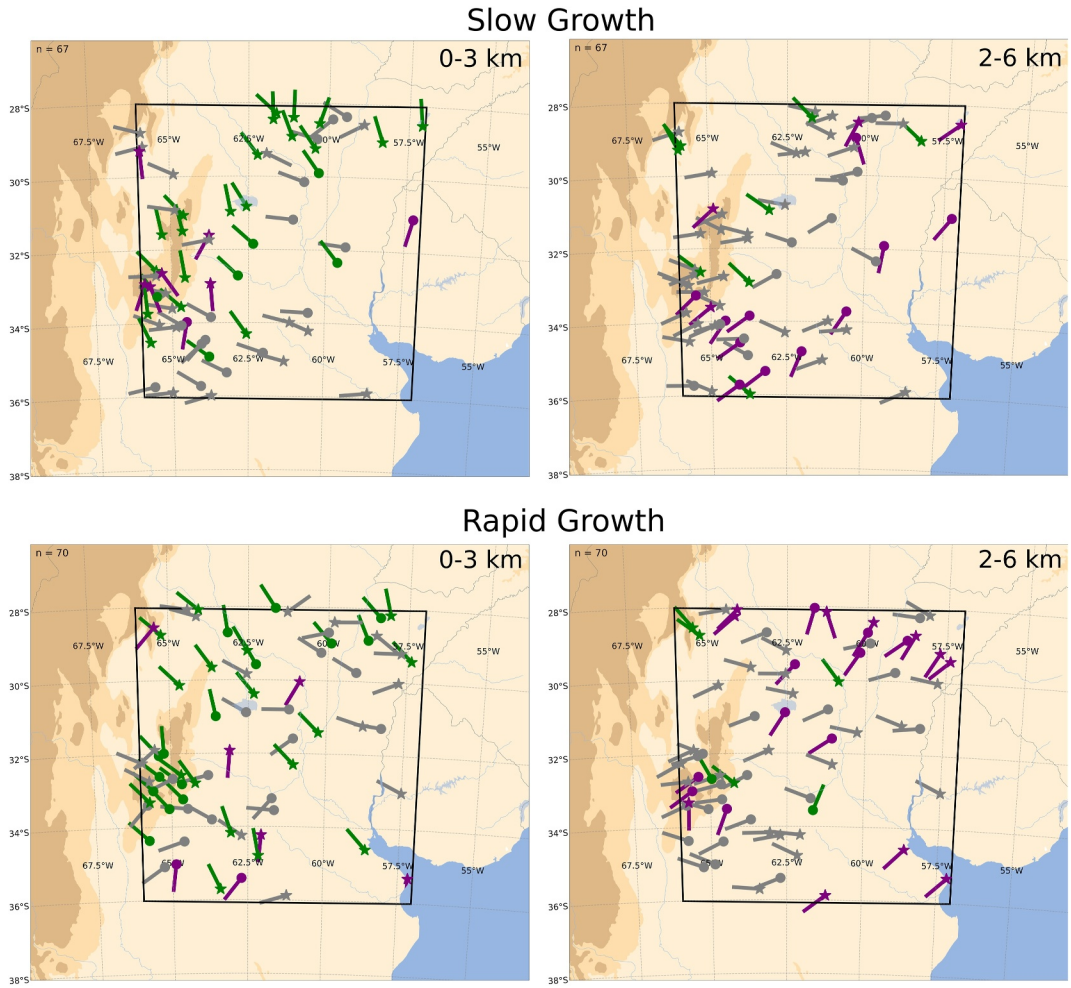

Figure 11. Maps of mesoscale convective system centroid locations separated by growth rate. The shape of the symbol indicates whether a South American Low-level Jet (SALLJ) was identified (circle: SALLJ, star: no SALLJ) and the color indicates the primary direction of the shear vector (green: North, purple: South, gray: East/West) for 0–3 km shear (left) and 2–6 km shear (right). Lines show the direction the shear is from as indicated with the colors (i.e., green lines are northerly shear). Terrain contours are as in Figures 1, 2 and 4.

low-level shear direction alone is not a predictor of growth rate. Similarly, there is not a clear isolated role of the SALLJ in leading to a favorable deep-layer (2-6-km) shear orientation (i.e., north-south) for rapid upscale growth of SDC-initiated convection, which is not a surprise given that the shear orientation is also strongly influenced by the relative strength and orientation of the 6-km winds that also vary throughout upscale growth events. This result suggests that the rapid growth near the SDC likely results from the combined thermodynamic and kinematic influences of the SALLJ.

Together, these results highlight the importance of the SALLJ to rapid upscale growth near the SDC. While the SALLJ can orient wind shear in a favorable direction for upscale growth, it also creates a thermodynamic environment that is very favorable for rapid growth MCSs.

4. Discussion and Conclusions

A 6.5-month convection-permitting WRF simulation with 3-km horizontal grid spacing was used to examine the characteristics and environments of developing MCSs in central Argentina, with the goal of exploring how local environmental differences relate to variations in the rate of spatial growth near the complex terrain of the SDC. The duration of the model run coupled with its ability to resolve mesoscale and topographic processes allows for a unique look into upscale growth environments near the SDC in central Argentina.

The "first storms" and "MCS initiation" locations are clustered near the southern end of the SDC and deep convection grows upscale to an MCS more rapidly and over a shorter distance than in the U.S. Specifically, most of the convection that forms over the higher terrain of the SDC (>500 m MSL) and grows upscale into an MCS, stays near the higher terrain during its initial upscale growth. The simulated storms rapidly transitioned to MCSs, similar to radar (Mulholland et al., 2018) and satellite (Zhang et al., 2021) observations, and the rapid growth MCSs occur more frequently during overnight hours likely related to the nocturnal acceleration of the SALLJ (Sasaki et al., 2022).

Comparing the distributions of mean environmental parameters at the "first storms" stage reveals statistically significant differences in the thermodynamic environment for rapid growth MCSs compared to slow growth MCSs. The thermodynamic environment, including CAPE and LFC-LCL height difference, is more favorable over a large spatial area, resulting in part from a more frequent and stronger SALLJ (Sasaki et al., 2024) during rapid growth MCSs compared to slow growth MCSs. Larger potential instability is found for rapid growth MCSs, which has been hypothesized to indicate an environment that is favorable for the rapid spatial growth of convection through slab lifting (Coniglio et al., 2010). This result is especially relevant in an environment with complex terrain and a LLJ as they could be common sources of strong lifting (e.g., French & Parker, 2010).

Spatially averaged vertical wind shear magnitudes were generally similar between slow and rapid growth MCSs, with a large spread in values. However, 0–2 km shear magnitude is an exception with greater magnitudes for rapid growth MCSs, which may be related to the more frequent presence of the SALLJ in these cases and thus influence on 2-km winds (see Figure S30 in Supporting Information S1). Further, elevated-layer (i.e., 2-6-km and 3-10-km) shear magnitudes did not differ significantly between slow versus rapid growth MCSs, but were smaller for very rapid growth compared to very slow growth MCSs. This result is in part attributed to stronger SALLJ winds for the very rapid growth MCSs reducing the wind speed difference with mid-level flow within the trough (e.g., Sasaki et al., 2025; Zhang et al., 2021). However, variable SALLJ strengths, orientations, and locations relative to the SDC, along with a wide variety of strengths and directions of mid-level flow observed within the simulated cases, leads to a large spread in environmental variables.

The lack of significant differences when comparing slow versus rapid growth inclusive of all cases is similar to past studies, which have shown mixed results regarding whether shear magnitude alone can be used to discriminate deep convective upscale growth occurrence and rate (Cohen et al., 2007; Coniglio et al., 2010; Hiris & Gallus, 2021; Hwang et al., 2022; Hwang and Li, 2022; Mulholland et al., 2018). However, both this study and prior work suggest that the orientation of the deep-layer shear vector relative to the low-level forcing, when considered alongside thermodynamic parameters, may be more effective in determining growth rate (Cohen et al., 2007; Coniglio et al., 2010, 2011; Sasaki et al., 2025). The presence of a SALLJ near the southern end of the SDC appears to be the best indicator of rapid growth, likely due to a combination of a favorable thermodynamic environment and wind shear orientation produced by the SALLJ (Sasaki et al., 2022, 2024, 2025), along with a potential local enhancement of shear due to the terrain (Singh et al., 2022). These findings emphasize an important role of the SALLJ, within favorable synoptic environments, in promoting rapid MCS development in the presence of complex terrain.

A limitation of this study is that only the environment at the "first storms" stage was compared, due to model biases later in the MCS lifecycle (Zhang et al., 2021). Further studies should compare environments throughout the period of growth to MCS to understand how the evolution of the environments may impact growth rate. However, as the convection grows upscale, convection contamination of the environmental conditions might need to be considered as well as MCS inflow regions once an MCS forms. Additionally, longer simulations with a larger sample of events could enable more detailed categorization of MCS environments based on factors such as SALLJ height, MCS type, and the initiating mechanism (e.g., terrain or frontal boundary). This approach would also allow for quantifying the frequency of varying synoptic patterns that contribute to these factors, recognizing that our approach of averaging environmental parameters over a 4° by 4° box limits our ability to fully disentangle local environmental conditions from broader synoptic influences. The spread of wind shear values within events further highlights the need to further explore the factors driving shear variability at sub-synoptic scales, particularly terrain influences. Such investigations are necessary to separate the influences of the many mechanisms controlling growth rates and further differentiate environments favorable for rapid growth under a variety of conditions.

Conflict of Interest

The authors declare no conflicts of interest relevant to this study.

Data Availability Statement

The MCS tracking data set along with the Python code used to generate figures for its analysis are available from Zenodo (Sasaki, 2025). For further details on the WRF model run from which the MCS tracking data set is derived, readers are referred to Zhang et al. (2021).

Acknowledgments
The authors are grateful to Stacy Brodzik for managing the data used in this analysis. This work has also benefited from helpful discussion with Kristen Rasmussen, Daniel Veloso-Águila, Anthony Bernal Ayala, and Mitchell Gregg. This research was supported by NSF Grants AGS-2146708 and AGS-2146710. Further support was provided by the U.S. Department of Energy Office of Science Biological and Environmental Research, through the Atmospheric System Research program. Pacific Northwest National Laboratory is operated by Battelle for the U.S. Department of Energy under Contract DE-AC05-76RLO1830. Computational and storage resources for the WRF simulation were provided by the NCAR Computational and Information Systems Laboratory, the University of Utah Center for High Performance Computing, and the National Energy Research Scientific Computing Center, a Department of Energy Office of Science User Facility, supported by the Office of Science of the U.S. Department of Energy under Contract DE-AC02-05CH11231.

References

Bennett, L. J., Browning, K. A., Blyth, A. M., Parker, D. J., & Clark, P. A. (2006). A review of the initiation of precipitating convection in the United Kingdom. *Quarterly Journal of the Royal Meteorological Society*, *132*(617), 1001–1020. https://doi.org/10.1256/qj.05.54

Browning, K. A., Blyth, A. M., Clark, P. A., Corsmeier, U., Morcrette, C. J., Agnew, J. L., et al. (2007). The convective storm initiation project. *Bulletin of the American Meteorological Society*, *88*(12), 1939–1955. https://doi.org/10.1175/BAMS-88-12-1939

Cohen, A. E., Coniglio, M. C., Corfidi, S. F., & Corfidi, S. J. (2007). Discrimination of mesoscale convective system environments using sounding observations. *Weather and Forecasting*, *22*(5), 1045–1062. https://doi.org/10.1175/WAF1040.1

Coniglio, M. C., Corfidi, S. F., & Kain, J. S. (2011). Environment and early evolution of the 8 May 2009 derecho-producing convective system. *Monthly Weather Review*, *139*(4), 1083–1102. https://doi.org/10.1175/2010MWR3413.1

Coniglio, M. C., Hwang, J. Y., & Stensrud, D. J. (2010). Environmental factors in the upscale growth and longevity of MCSs derived from rapid update cycle analyses. *Monthly Weather Review*, *138*(9), 3514–3539. https://doi.org/10.1175/2010MWR3233.1

Crook, N. A., & Moncrieff, M. W. (1988). The effect of large-scale convergence on the generation and maintenance of deep moist convection. *Journal of the Atmospheric Sciences*, *45*(23), 3606–3624. https://doi.org/10.1175/1520-0469(1988)045<3606:teolsc>2.0.co;2

Davies, J. M. (2004). Total cape, low-level CAPE, and LFC in significant tornado events with relatively high LCL heights. In *Paper presented at 23rd conference on severe local storms*. American Meteorological Society. Retrieved from https://ams.confex.com/ams/pdfpapers/115481.pdf

Dial, G. L., Racy, J. P., & Thompson, R. L. (2010). Short-term convective mode evolution along synoptic boundaries. *Weather and Forecasting*, *25*(5), 1430–1446. https://doi.org/10.1175/2010WAF2222315.1

Du, Y., Chen, G., Han, B., Bai, L., & Li, M. (2020). Convection initiation and growth at the Coast of south China. Part II: Effects of the terrain, coastline, and cold pools. *Monthly Weather Review*, *148*(9), 2871–3892. https://doi.org/10.1175/MWR-D-20-0090.1

Du, Y., Zhang, Q., Chen, Y.-L., Zhao, Y., & Wang, X. (2014). Numerical simulations of spatial distributions and diurnal variations of low-level jets in China during early summer. *Journal of Climate*, *27*(15), 5747–5767. https://doi.org/10.1175/JCLI-D-13-00571.1

Feng, Z., Hardin, J., Barnes, H. C., Li, J., Leung, L. R., Varble, A., & Zhang, Z. (2023). PyFLEXTRKR: A flexible feature tracking python software for convective cloud analysis. *Geoscientific Model Development*, *16*(10), 2753–2776. https://doi.org/10.5194/gmd-16-2753-2023

Feng, Z., Prein, A. F., Kukulies, J., Fiolleau, T., Jones, W. K., Maybee, B., et al. (2025). Mesoscale convective systems tracking method intercomparison (MCSMIP): Application to DYAMOND global km-Scale simulations. *Journal of Geophysical Research: Atmospheres*, *130*(8), 1–29. https://doi.org/10.1029/2024JD042204

Feng, Z., Varble, A., Hardin, J., Marquis, J., Hunzinger, A., Zhang, Z., & Thieman, M. (2022). Deep convection initiation, growth, and environments in the complex terrain of central Argentina during CACTI. *Monthly Weather Review*, *150*(5), 1135–1155. https://doi.org/10.1175/MWR-D-21-0237.1

French, A. J., & Parker, M. D. (2010). The response of simulated nocturnal convective systems to a developing low-level jet. *Journal of the Atmospheric Sciences*, *67*(10), 3384–3408. https://doi.org/10.1175/2010JAS3329.1

Gallus, W. A., Snook, N. A., & Johnson, E. V. (2008). Spring and summer severe weather reports over the midwest as a function of convective mode: A preliminary study. *Weather and Forecasting*, *23*(1), 101–113. https://doi.org/10.1175/2007WAF2006120.1

Garcia, D. W., Reboita, M. S., & Mattos, E. V. (2024). Lifting condensation level climatology over South America. *Revista Brasileira de Geografia Fisica*, *17*(2), 895–913. https://doi.org/10.26848/rbgf.v17.2.p895-913

Hartmann, D. L., Hendon, H. H., & Houze, R. A. (1984). Some implications of the mesoscale circulations in tropical cloud clusters for large-scale dynamics and climate. *Journal of the Atmospheric Sciences*, *41*(1), 113–121. https://doi.org/10.1175/1520-0469(1984)041<0113:SIOTMC>2.0.CO;2

Hersbach, H., & Coauthors. (2020). The ERA5 global reanalysis. *Quart. J. Roy. Meteor. Soc.*, *146*, 1999–2049. https://doi.org/10.1002/qj.3803

Hiris, Z. A., & Gallus, W. A. (2021). On the relationship of cold pool and bulk shear magnitudes on upscale convective growth in the Great Plains of the United States. *Atmosphere*, *12*(8), 1019. https://doi.org/10.3390/atmos12081019

Hwang, Y., & Li, Y. (2022). Characteristics of the daytime and nighttime MCSs over the Canadian prairies using an ERA5-forced convection-permitting climate model. *Atmospheric Research*, *279*(July), 106380. https://doi.org/10.1016/j.atmosres.2022.106380

Hwang, Y., Li, Z., & Li, Y. (2022). Features of MCSs in the central United States using simulations of ERA5-Forced convection-permitting climate models. *Weather and Forecasting*, *37*(9), 1681–1702. https://doi.org/10.1175/WAF-D-22-0022.1

Iacono, M. J., Delamere, J. S., Mlawer, E. J., Shepard, M. W., Clough, S. A., & Collins, W. D. (2008). Radiative forcing by longwave greenhouse gases: Calculations with the AER radiative transfer models. *Journal of Geophysical Research*, *113*, D13103. https://doi.org/10.1029/2008JD009944

Janjić, Z. I. (1994). The step-mountain eta coordinate model: Further developments of the convection, viscous sublayer, and turbulence closure schemes. *Monthly Weather Review*, *122*(5), 927–945. https://doi.org/10.1175/1520-0493(1994)122<0927:TSMECM>2.0.CO;2

Jirak, I. L., & Cotton, W. R. (2007). Observational analysis of the predictability of mesoscale convective systems. *Weather and Forecasting*, *22*(4), 813–838. https://doi.org/10.1175/WAF1012.1

Kang, S. L., & Bryan, G. H. (2011). A large-eddy simulation study of moist convection initiation over heterogeneous surface fluxes. *Monthly Weather Review*, *139*(9), 2901–2917. https://doi.org/10.1175/MWR-D-10-05037.1

Ladwig, W. (2017). wrf-python [Software]. *UCAR/NCAR*. https://doi.org/10.5065/D6W094P1

Maddox, R. A., Chappell, C. F., & Hoxit, L. R. (1979). Synoptic and Meso-a scale aspects of flash flood events. *Bulletin of the American Meteorological Society*, *60*(2), 115–123. https://doi.org/10.1175/1520-0477-60.2.115

Monin, A. S., & Obukhov, A. M. (1954). Basic laws of turbulent mixing in the surface layer of the atmosphere. *Contrib. Geophys. Inst. Acad. Sci. USSR*, *151*, 163–187.

Mulholland, J. P., Nesbitt, S. W., & Trapp, R. J. (2019). A case study of terrain influences on upscale convective growth of a supercell. *Monthly Weather Review*, *147*(12), 4305–4324. https://doi.org/10.1175/MWR-D-19-0099.1

Mulholland, J. P., Nesbitt, S. W., Trapp, R. J., Rasmussen, K. L., & Salio, P. V. (2018). Convective storm life cycle and environments near the Sierras de Córdoba, Argentina. *Monthly Weather Review*, *146*(8), 2541–2557. https://doi.org/10.1175/MWR-D-18-0081.1

Mulholland, J. P., Peters, J. M., & Morrison, H. (2021). How does LCL height influence deep convective updraft width? *Geophysical Research Letters*, *48*(13), 1–8. https://doi.org/10.1029/2021GL093316

Nakanishi, M., & Niino, H. (2006). An improved mellor–yamada Level-3 model: Its numerical stability and application to a regional prediction of advection fog. *Bound.-Layer Meteor.*, *119*(2), 397–407. https://doi.org/10.1007/s10546-005-9030-8

Nakanishi, M., & Niino, H. (2009). Development of an improved turbulence closure model for the atmospheric boundary layer. *J. Meteor. Soc. Japan*, *87*(5), 895–912. https://doi.org/10.2151/jmsj.87.895

Nesbitt, S. W., Salio, P. V., Ávila, E., Bitzer, P., Carey, L., Chandrasekar, V., et al. (2021). A storm safari in subtropical South America: Proyecto RELAMPAGO. *Bulletin of the American Meteorological Society*, *102*(8), E1621–E1644. https://doi.org/10.1175/BAMS-D-20-0029.1

Nicolini, M., Salio, P., Ulke, G., Marengo, J., Douglas, M., Paegle, J., & Zipser, E. (2004). South American low-level jet diurnal cycle and three dimensional structure. *CLIVAR Exchanges, No. 9, International CLIVAR Project Office*, 6–8.

Peters, J. M., Eure, K. C., & Schumacher, R. S. (2017). Factors that drive MCS growth from supercells. In *Paper presented at 17th conference on mesoscale processes*. American Meteorological Society. Retrieved from https://ams.confex.com/ams/17MESO/webprogram/Paper320248.html

Peters, J. M., & Schumacher, R. S. (2014). Objective categorization of heavy-rain-producing MCS synoptic types by rotated principal component analysis. *Monthly Weather Review*, *142*(5), 1716–1737. https://doi.org/10.1175/MWR-D-13-00295.1

Piscitelli, F. M., Ruiz, J. J., Negri, P., & Salio, P. (2022). A multiyear radar-based climatology of supercell thunderstorms in central-eastern Argentina. *Atmospheric Research*, *277*(February), 106283. https://doi.org/10.1016/j.atmosres.2022.106283

Rasmussen, K. L., & Houze, R. A. (2011). Orogenic convection in subtropical South America as seen by the TRMM satellite. *Monthly Weather Review*, *139*(8), 2399–2420. https://doi.org/10.1175/MWR-D-10-05006.1

Rasmussen, K. L., & Houze, R. A. (2016). Convective initiation near the andes in subtropical South America. *Monthly Weather Review*, *144*(6), 2351–2374. https://doi.org/10.1175/MWR-D-15-0058.1

Rasmusson, E. M., & Mo, K. C. (1996). Large-scale atmospheric moisture cycling as evaluated from NMC global analysis and forecast products. *Journal of Climate*, *9*(12), 3276–3297. https://doi.org/10.1175/1520-0442(1996)009<3276:LSAMCA>2.0.CO;2

Ribeiro, B. Z., & Bosart, L. F. (2018). Elevated mixed layers and associated severe thunderstorm environments in south and North America. *Monthly Weather Review*, *146*(1), 3–28. https://doi.org/10.1175/MWR-D-17-0121.1

Rocque, M. N., & Rasmussen, K. L. (2022). The impact of topography on the environment and life cycle of weakly and strongly forced MCSs during RELAMPAGO. *Monthly Weather Review*, *150*(9), 2317–2338. https://doi.org/10.1175/MWR-D-22-0049.1

Rotunno, R., Klemp, J. B., & Weisman, M. L. (1988). A theory for strong, long-lived squall lines. *Journal of the Atmospheric Sciences*, *45*(3), 463–485. https://doi.org/10.1175/1520-0469(1988)045<0463:atfsll>2.0.co;2

Russell, A., Vaughan, G., Norton, E. G., Morcrette, C. J., Browning, K. A., & Blyth, A. M. (2008). Convective inhibition beneath an upper-level PV anomaly. *Quarterly Journal of the Royal Meteorological Society*, *134*(631 PART B), 371–383. https://doi.org/10.1002/qj.214

Salio, P., Nicolini, M., & Zipser, E. J. (2007). Mesoscale convective systems over southeastern South America and their relationship with the south American low-level jet. *Monthly Weather Review*, *135*(4), 1290–1309. https://doi.org/10.1175/MWR3305.1

Sasaki, C. (2025). ClaytonSasaki/WRF_Upscale_Growth_Paper: Data and Code for "Environmental Influences on Deep Convective Upscale Growth Rate in Central Argentina from a Convection-Permitting Simulation" by Sasaki et al. (2025) (v1.0.0) [Dataset, Software]. *Zenodo*. https://doi.org/10.5281/zenodo.15272277

Sasaki, C. R. S., Rowe, A. K., & McMurdie, L. A. (2025). Environmental conditions leading to observed convective organization in central Argentina. *Monthly Weather Review*, *153*(11), 2415–2435. https://doi.org/10.1175/MWR-D-24-0183.1

Sasaki, C. R. S., Rowe, A. K., McMurdie, L. A., & Rasmussen, K. L. (2022). New insights into the south American low-level jet from RELAMPAGO observations. *Monthly Weather Review*, *150*(6), 1247–1271. https://doi.org/10.1175/MWR-D-21-0161.1

Sasaki, C. R. S., Rowe, A. K., McMurdie, L. A., Varble, A. C., & Zhang, Z. (2024). Influences of the south American low-level jet on the convective environment in central Argentina using a convection-permitting simulation. *Monthly Weather Review*, *152*(2), 629–648. https://doi.org/10.1175/MWR-D-23-0122.1

Schumacher, R. S., & Coauthors. (2021). Convective-storm environments in subtropical South America from high-frequency soundings during RELAMPAGO-CACTI. *Monthly Weather Review*, *149*, 1439–1458. https://doi.org/10.1175/MWR-D-20-0293.1

Schumacher, R. S., & Johnson, R. H. (2005). Organization and environmental properties of extreme-rain-producing mesoscale convective systems. *Monthly Weather Review*, *133*(4), 961–976. https://doi.org/10.1175/MWR2899.1

Singh, I., Nesbitt, S. W., & Davis, C. A. (2022). Quasi-Idealized Numerical Simulations of Processes Involved in Orogenic Convection Initiation over the Sierras de Córdoba. *Journal of the Atmospheric Sciences*, *79*(4), 1127–1149. https://doi.org/10.1175/JAS-D-21-0007.1

Skamarock, W., Klemp, J., Dudhia, J., Gill, D. O., Liu, Z., Berner, J., et al. (2019). *A description of the advanced research WRF model version 4.1*. Note NCAR/TN-5561STR. https://doi.org/10.5065/1dfh-6p97

Smith, B. T., Thompson, R. L., Grams, J. S., Broyles, C., & Brooks, H. E. (2012). Convective modes for significant severe thunderstorms in the contiguous United States. Part I: Storm classification and climatology. *Weather and Forecasting*, *27*(5), 1114–1135. https://doi.org/10.1175/WAF-D-11-00115.1

Tao, W.-K., & Simpson, J. (1984). Cloud interactions and merging: Numerical simulations. *Journal of the Atmospheric Sciences*, *41*(19), 2901–22917. https://doi.org/10.1175/1520-0469(1984)041<2901:CIAMNS>2.0.CO;2

Tewari, M., & Coauthors. (2004). Implementation and verification of the unified Noah land surface model in the WRF model. In *20th conf. On weather analysis and forecasting, 16th conf. On numerical weather prediction* (Vol. 14.2a). Amer. Meteor. Soc. Retrieved from https://ams.confex.com/ams/84Annual/techprogram/paper_69061.htm

Thielen, J. E., & Gallus, W. A. (2019). Influences of horizontal grid spacing and microphysics on WRF forecasts of convective morphology evolution for nocturnal MCSs in weakly forced environments. *Weather and Forecasting*, *34*(5), 1495–1517. https://doi.org/10.1175/WAF-D-18-0210.1

Thompson, G., & Eidhammer, T. (2014). A study of aerosol impacts on clouds and precipitation development in a large winter cyclone. *Journal of the Atmospheric Sciences*, *71*(10), 3636–3658. https://doi.org/10.1175/JAS-D-13-0305.1

Thompson, R. L., Smith, B. T., Grams, J. S., Dean, A. R., & Broyles, C. (2012). Convective modes for significant severe thunderstorms in the contiguous United States. Part II: Supercell and QLCS tornado environments. *Weather and Forecasting*, *27*(5), 1136–1154. https://doi.org/10.1175/WAF-D-11-00116.1

Trapp, R. J., Kosiba, K. A., Marquis, J. N., Kumjian, M. R., Nesbitt, S. W., Wurman, J., et al. (2020). Multiple-platform and multiple-doppler radar observations of a supercell thunderstorm in South America during relampago. *Monthly Weather Review*, *148*(8), 3225–3241. https://doi.org/10.1175/MWR-D-20-0125.1

Trapp, R. J., Tessendorf, S. A., Godfrey, E. S., & Brooks, H. E. (2005). Tornadoes from squall lines and bow echoes. Part I: Climatological distribution. *Weather and Forecasting*, *20*(1), 23–34. https://doi.org/10.1175/WAF-835.1

Uccellini, L. W., & Johnson, D. R. (1979). On the role of upper tropospheric jet streaks and leeside cyclogenesis in the development of low-level jets in the great plains. *Monthly Weather Review*, *108*(10), 1689–1696.

Varble, A. C., Nesbitt, S. W., Salio, P., Hardin, J. C., Bharadwaj, N., Borque, P., et al. (2021). Utilizing a storm-generating hotspot to study convective cloud transitions: The CACTI experiment. *Bulletin of the American Meteorological Society*, *102*(8), E1597–E1620. https://doi.org/10.1175/BAMS-D-20-0030.1

Weisman, M. L., Evans, C., & Bosart, L. (2013). The 8 May 2009 superderecho: Analysis of a real-time explicit convective forecast. *Weather and Forecasting*, *28*(3), 863–892. https://doi.org/10.1175/WAF-D-12-00023.1

Weisman, M. L., & Rotunno, R. (2004). "A theory for strong long-lived squall lines" revisited. *Journal of the Atmospheric Sciences*, *61*(4), 361–382. https://doi.org/10.1175/1520-0469(2004)061<0361:ATFSLS>2.0.CO;2

Wu, Y., & Raman, S. (1998). The summertime great plains low level jet and the effect of its origin on moisture transport. *Boundary-Layer Meteorology*, *88*(3), 445–466. https://doi.org/10.1023/A:1001518302649

Zhang, Z., Varble, A., Feng, Z., Hardin, J., & Zipser, E. (2021). Growth of mesoscale convective systems in observations and a seasonal convection-permitting simulation over Argentina. *Monthly Weather Review*, *149*(10), 3469–3490. https://doi.org/10.1175/MWR-D-20-0411.1

Zhang, Z., Varble, A. C., Feng, Z., Marquis, J. N., Hardin, J. C., & Zipser, E. J. (2024). Dependencies of simulated convective cell and system growth biases on atmospheric instability and model resolution. *Journal of Geophysical Research: Atmospheres*, *129*(22), e2024JD041090. https://doi.org/10.1029/2024JD041090